Fabrication and Optical Probing of Highly Extended, Ultrathin Graphene Nanoribbons in Carbon Nanotubes

Hong En Lim,[†] Yasumitsu Miyata,[‡,§] Miho Fujihara,[†] Susumu Okada,[⊥] Zheng Liu,[∥] Arifin,[†] Kayoko Sato,[∥] Haruka Omachi,[†] Ryo Kitaura,[†] Stephan Irle,[†,#] Kazu Suenaga,[∥] and Hisanori Shinohara*[,†,○]

[†]Department of Chemistry, Nagoya University, Nagoya 464-8602, Japan, [‡]Department of Physics, Tokyo Metropolitan University, Hachioji 192-0397, Japan, [§]JST, PRESTO, Kawaguchi 332-0012, Japan, [⊥]Graduate School of Pure and Applied Sciences, University of Tsukuba, Tsukuba 305-8571, Japan, [∥]Nanotube Research Center, National Institute of Advanced Industrial Science and Technology (AIST), Tsukuba 305-8565, Japan, [#]WPI-Institute of Transformative Bio-Molecules (ITbM), Nagoya University, Nagoya 464-8602, Japan, and [○]Institute for Advanced Research, Nagoya University, Nagoya 464-8602, Japan

ABSTRACT Nanotemplated growth of graphene nanoribbons (GNRs) inside carbon nanotubes is a promising mean to fabricate ultrathin ribbons with desired side edge configuration. We report the optical properties of the GNRs formed in single-wall carbon nanotubes. When coronene is used as the precursor, extended GNRs are grown *via* a high-temperature annealing at 700 °C. Their optical responses are probed through the diazonium-based side-wall functionalization, which effectively suppresses the excitonic absorption peaks of the nanotubes without damaging the inner GNRs. Differential absorption spectra clearly show two distinct peaks around 1.5 and 3.4 eV. These peaks are assigned to the optical transitions between the van Hove singularities in the density of state of the GNRs in qualitative agreement with the first-principles calculations. Resonance Raman spectra and transmission electron microscope observations also support the formation of long GNRs.

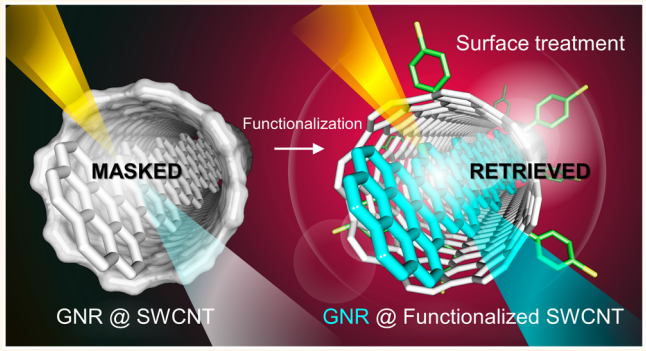

KEYWORDS: graphene nanoribbons · single-wall carbon nanotubes · functionalization · optical absorption

Ultrathin graphene nanoribbons (GNRs), the carbon strips with width of less than 2 nm, have been drawing much attention due to their unique electronic and optical properties.[1−6] The fact that their band gaps vary with width and side edge configuration[7−10] provides a great degree of freedom to manipulate their electronic structures and thus the optical responses, making them as one of the desirable materials for future nanoelectronics. Among the various synthetic approaches,[11−15] fabricating GNRs by using the bottom-up methods[16−18] is usually preferred so as to achieve extreme narrow width with edge uniformity.

The nanotemplated growth[18−20] in particular, where the GNRs are generated through the fusion of precursor molecules inserted into the template carbon nanotubes,[21−23] is one of the useful methods in fabricating ultrathin GNRs. There are vast varieties of the precursors and nanotubes available. Ribbons comprising of different sizes, edge structures and dopant atoms can be possibly designed with an appropriate choice of combination. Besides, the inert interior space allows the construction of novel ribbon structures, which may otherwise be unstable under ambient conditions.

In spite of these, the presence of the outer nanotubes oftentimes complicates the characterization of the inherent properties of GNRs encapsulated. The overall optical absorption characteristics of GNR@nanotubes, for instance, is predominated in features by those of the template nanotubes.[6] Signals generated by the inner ribbons are masked by a series of excitonic transition peaks, which extend over a broad range from UV to NIR region.[24] In this sense, it is necessary either to extract and isolate the inner GNRs out of the nanotubes or to eliminate the signals due to the template

* Address correspondence to noris@nagoya-u.jp.

Received for review December 27, 2014 and accepted April 13, 2015.

Published online April 13, 2015
10.1021/nn507408m

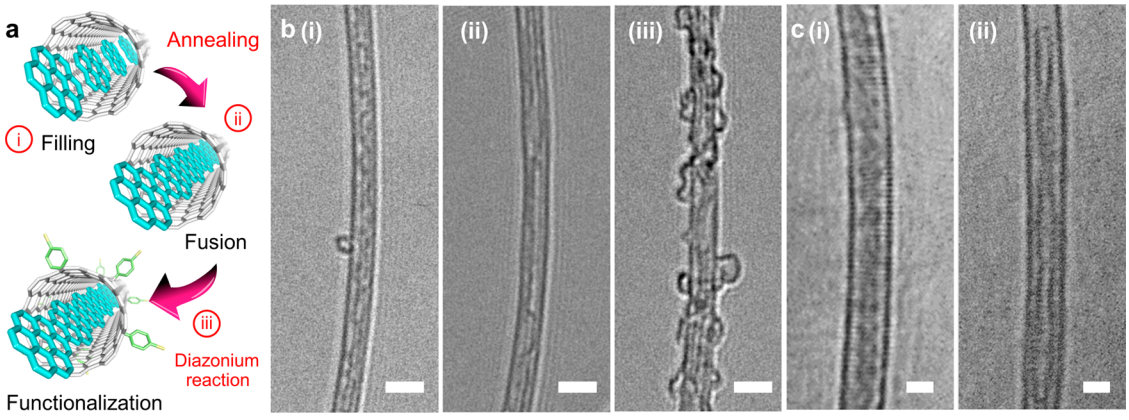

Figure 1. (a) The overall reaction scheme, starting with (i) the introduction of coronene precursors into the template SWCNTs, followed by (ii) the coalescence of the molecules encapsulated and finally, (iii) the surface modification of the outer side wall by diazonium chemistry. (b) The corresponding HRTEM images of the products formed at each stages in (a). Scale bars = 2 nm. (c) Typical C_s-HRTEM images of the L-GNR@SWCNTs showing the (i) horizontal and (ii) perpendicular orientations of the inner GNRs. Scale bars = 1 nm.

nanotubes. The former has not been done so far, as it entails vigorous sonication[20,25] that would at the same time cause damages to the GNRs synthesized once they are exposed to solutions. Under such circumstances, the latter is more feasible. One of the most promising ways to achieve this involves covalent functionalizations,[26−29] which disrupt the π-conjugated network of the outer side wall while keeping the inner materials intact. It is an effective technique that has been widely applied in the studies of the electrical and optical properties of the inner tubes of double-wall carbon nanotubes.[30,31]

Here, we report the intrinsic optical properties of the GNRs prepared in the interior space of single-wall carbon nanotubes (SWCNTs) of 1.4−1.6 nm in diameter. The ribbons were generated through the polymeric reaction of coronene molecules that took place under high-temperature annealing. With the use of the diazonium chemistry, the electronic states of the outer nanotubes were modified through surface functionalization, which enabled us to obtain distinct optical responses of the inner GNRs. We observed the intense optical absorption peaks around 1.5 and 3.4 eV, which coincide qualitatively with those predicted by the first-principles calculations. The present study sheds important light on the physical properties of the ultrathin GNRs residing in the confined state of SWCNTs, and thereby, contributing to their future applications in electronics and optoelectronics.

RESULTS AND DISCUSSION

The overall reaction scheme and the high resolution transmission electron microscope (HRTEM) images of the respective products formed are shown in Figure 1a and b, respectively. Coronene is selected as the precursor because of its high filling yield in the SWCNTs and its high reactivity. It can be easily turned into its dimeric form during the encapsulation process, to give a mixture of dimers and other linearly condensed coronene oligomers, which can also be regarded as short GNRs (S-GNRs), inside the template nanotubes.[22] In this work, instead of mere filling, the resulting samples are heated at 700 °C, to induce further polymerization/fusion reactions into the long GNRs (L-GNRs). The products obtained before and after annealing are thereafter termed, S-GNR@SWCNTs and L-GNR@SWCNTs, respectively, to aid the description in the following text.

The transformation of S-GNR@SWCNTs into the L-GNR@SWCNTs can be visualized in Figure 1b(i),(ii),c, and Supporting Information Figure S1. Densely packed, segmented structures of coronene dimers and oligomers, which align themselves at the center cavity of the SWCNT (Figure 1b(i)), are converted into linear, chain-like structures of long length (Figure 1b(ii)). The structural details for the L-GNRs formed can be clearly seen from the images taken under aberration corrected (C_s)-HRTEM in Figure 1c. Good correlations are found between the images in Figure 1c(i) with those of Supporting Information Figure S2(ii),(iii) and Supporting Information Figure S3(ii),(iii); while Figure 1c(ii) could be any of those in Supporting Information Figure S2(iv),(v) and Supporting Information Figure S3(iv),(v). Matching these observations to the simulated images strongly suggests that the GNRs indeed adopt a bilayer stacking in the CNTs. The subsequent reaction with 4-bromobenzene diazonium tetrafluoroborate (Scheme 1) grafted aryl groups onto the outer nanotubes. Intensive surface modification leads to Figure 1b(iii), where the resulting nanotubes are covered with amorphous-like impurities[27] that probably formed as a consequence of the diazonium radical side reaction.[28]

The extension of the GNRs can be traced by observing the change in their respective Raman spectra obtained before (S-GNR@SWCNTs) and after high

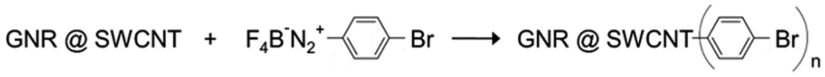

Scheme 1. Functionalization of GNR@SWCNTs with 4-bromobenzenediazonium tetrafluoroborate.

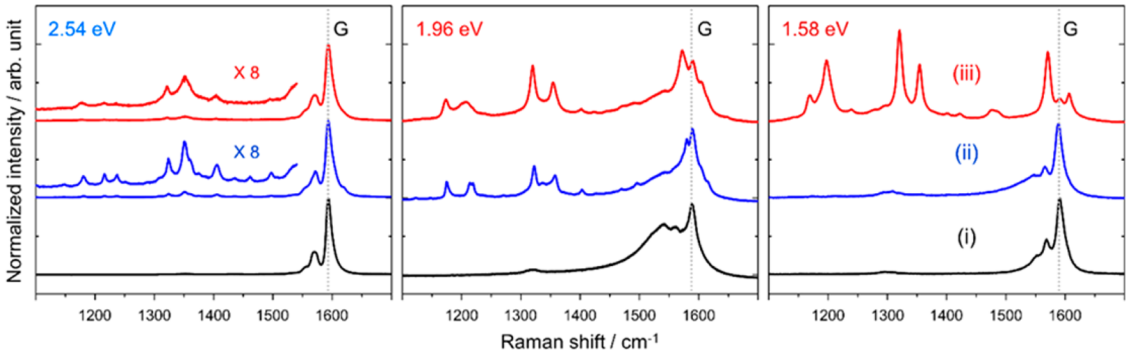

Figure 2. Raman spectra of the (i) pristine SWCNTs (black), (ii) S-GNR@SWCNTs (blue) and (iii) L-GNR@SWCNTs (red), recorded at 2.54, 1.96, and 1.58 eV, respectively.

temperature annealing (L-GNR@SWCNTs) as shown in Figure 2. Both samples display similar spectral features in general at 2.54 and 1.96 eV excitations. The triple-peak profile at 1323, 1350, and 1405 cm^{-1} (2.54 eV) and the double-peak profile at 1322 and 1357 cm^{-1} (1.96 eV) can be assigned respectively to those of the encapsulated coronene dimers and its oligomers, which form simultaneously under the present filling conditions as discussed in detail in our previous study.[22]

An entirely different spectrum is observed, however, at 1.58 eV excitation. The annealed sample shows intense peaks at 1150−1370 cm^{-1}, which are totally absent prior to annealing. The new features resemble those in 1.96 eV with an obvious down shift (~5 cm^{-1}) of peaks at 1160−1240 cm^{-1} (Supporting Information Figure S4), which are consistent with the theoretical predictions on the formation of the more extended GNRs with well-defined structures of armchair conformation.[22] We note that these Raman spectra are much different from the simulated Raman spectra of similar GNR systems with zigzag edges (Supporting Information Figures S5 and S6). This is reasonable because the present GNR formation is caused by thermally induced polymerization of dicoronylene molecules, which are formed during the vapor-phase encapsulation process of coronene molecules, as reported in our previous work.[22] Before the heat treatment, no characteristic peaks of the inner compounds are detected in the S-GNR@SWCNTs as it consists mainly molecules of short fragments. Upon the annealing at 700 °C, the structural confinement exerted by the template nanotubes causes the precursors inside to undergo an extensive polymerization with the neighboring molecules. The π-extension results in the observation of nanoribbons, which eventually come into strong resonance at a lower energy while maintaining the general Raman peaks profile in consistent with the HRTEM observations.

The respective optical absorption spectra of the pristine samples of SWCNTs, S-GNR@SWCNTs, and L-GNR@SWCNTs are shown in Figure 3a. In comparison with the empty nanotubes, there is a notable increase in the absorption of L-GNR@SWCNTs at the M_{11} region. As in previous studies on fullerenes/stacked-coronene/GNR-filled CNTs samples,[6,32,33] their spectral features are dominated basically by those of the template nanotubes. Only limited information can be obtained regarding the compounds situated inside. The reaction with 4-bromobenzene diazonium tetrafluoroborate provides a clear window to examine the inner products formed as in Figure 3b. Functionalization of the aryl groups yielded a featureless spectrum in the reference SWCNTs sample. The characteristic excitonic peaks of the outer nanotubes are almost completely removed, and signals due to the inner compounds start to appear as seen in Figure 3b. Subtracting the reference spectrum from each corresponding spectra of S-GNR@SWCNTs and L-GNR@SWCNTs provides the differential absorption spectra in Figure 3c,d. In Figure 3c, the spectra have low signal-to-noise ratio with additional spikes because the presence of inner compounds modulates the excitonic peaks of outer CNTs. It is therefore difficult to subtract only the SWCNTs contributions from the spectra of GNR@SWCNTs. This difficulty can be overcome through the suppression of the excitonic peaks by functionalization as shown in Figure 3d. The difference in the absorption spectra between S-GNR@SWCNTs and L-GNR@SWCNTs is rather prominent: the former shows absorption bands around 2.4 and 3.5 eV, whereas the latter shows bands around 1.5 and 3.4 eV.

The absorption bands in S-GNR@SWCNTs are attributable to those of coronene dimer, the dicoronylene (2.48, 2.63, 3.47 eV).[34] They are easily transformed into much polymerized forms by the high-temperature annealing in the L-GNR@SWCNTs. This is evidenced by the fact that

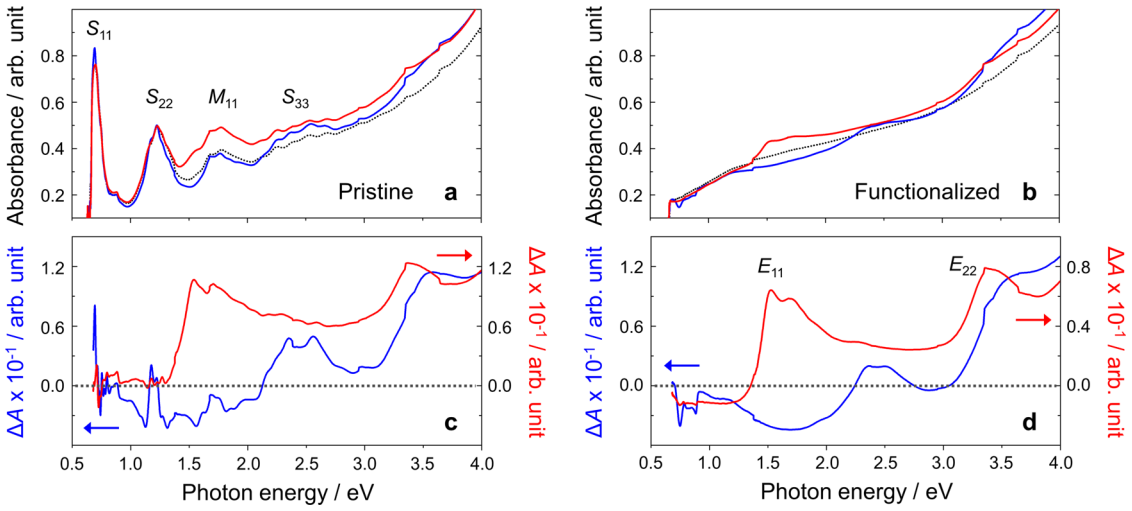

Figure 3. Optical absorption spectra of the (a) pristine and (b) functionalized samples of SWCNTs (black), S-GNR@SWCNTs (blue) and L-GNR@SWCNTs (red). Spectral features due to the radical side reaction (Supporting Information Figure S7) are subtracted from the spectra in (b) for clarity. Differential absorption spectra of the (c) pristine and (d) functionalized samples, obtained by subtracting the spectrum of SWCNTs from those of S-GNR@SWCNTs (blue) and L-GNR@SWCNTs (red) in panels (a) and (b).

the absorption band appears in the lower energy region[35] together with the on state resonance Raman spectrum at 1.58 eV excitation as shown in Figure 2.

To obtain information on the absorption bands seen in Figure 3d, the electronic structure of the GNR was computed. Because both the experimental and theoretical Raman spectra comply well with each other, the calculations were thereby, performed on an infinitely long, coronene-derived GNR (Figure 4a), using the density functional theory (DFT) with the local density approximation (LDA). The energy gap between the highest occupied and the lowest unoccupied states (E_{11}) and the gap between the second highest occupied and the second lowest unoccupied states (E_{22}) at the Γ point in Figure 4b are estimated to be 0.8 and 3.1 eV, respectively. Since DFT-LDA usually underestimates the fundamental energy gap of semiconducting materials because of the lack of the self-interaction energies, the computed E_{11} value has to be corrected by a multiplication of some factors.[36,37] Thus, the computed values of 0.8 and 3.1 eV are in qualitatively good agreement with the experimentally observed bands in Figure 3c, suggesting the formation of coronene-ribbons with long length. Nevertheless, as reported by Denk and Prezzi *et al.*,[5,38] a quasi one-dimensional system like this involves a more complicated optical transitions due to the strong electron–hole interactions. Further in depth studies are required to ascribe the transitions quantitatively, taking the excitonic effects into consideration.

The formation of long GNRs within SWCNTs can be justified when we follow the evolution in the absorption and Raman spectra of the L-GNR@SWCNTs during the reaction with diazonium salt. As the reaction proceeds, the excitonic peaks of the template nanotubes gradually decrease until they are fully depleted

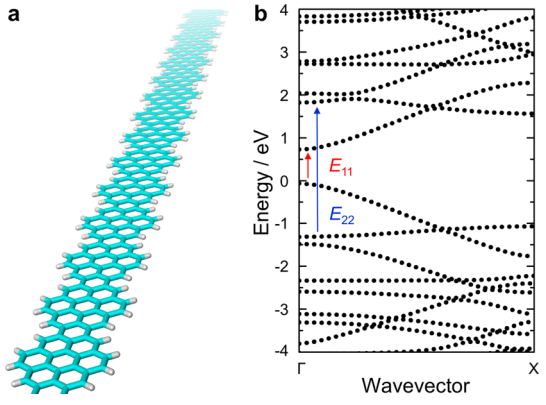

Figure 4. (a) Structure model of the infinitely long GNR used for the DFT calculation. Blue, carbon atoms; white, hydrogen atoms. (b) Computed band structure of (a).

(Figure 5a and Supporting Information Figure S7). This is accompanied by a simultaneous increase in the D-band and a sudden decrease in the radial breathing modes (RBM) of the Raman spectra (at 1.96 and 2.54 eV) as shown in Supporting Information Figures S8 and S9, which strongly suggest the presence of the so-called sp^3-defects inflicted onto the nanotubes. The outer nanotubes are considered to be highly functionalized when the D-band reaches its maximum on the fourth day together with the complete disappearance of their corresponding peaks in RBM region.

The absorption of the encapsulated GNRs, in contrast, which appears initially as a shoulder around 1.5 eV, remains relatively unchanged throughout the reaction. In reference to the Raman spectra taken for the pristine and functionalized sample at 1.58 eV (Figure 5b), where the GNRs are in strong resonance, the GNRs peaks are kept intact, while the RBM and G bands of the template nanotubes are no longer observed.

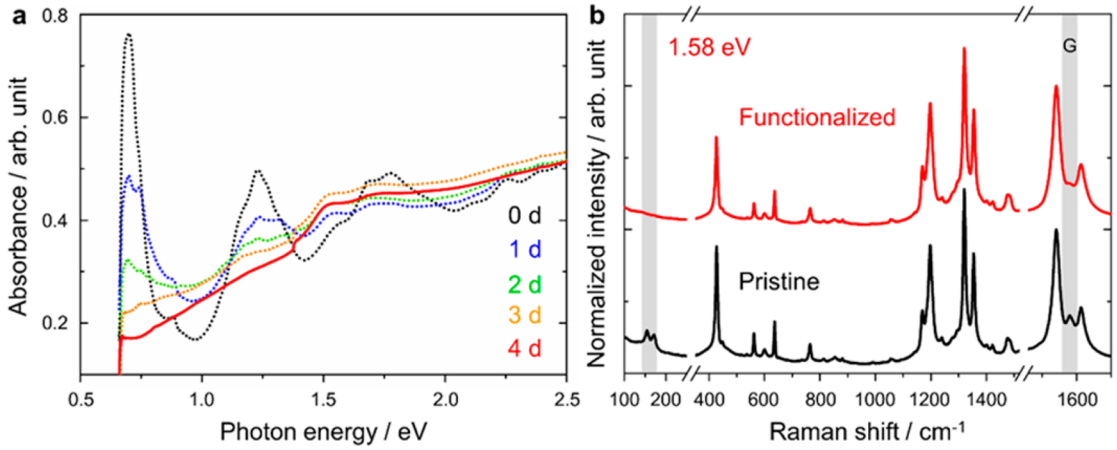

Figure 5. (a) Evolution of the optical absorption spectra of the L-GNR@SWCNTs in the course of reaction with 10 mM diazonium solution over a period of 4 days. Spectral features due to the radical side reaction (Supporting Information Figure S7) are subtracted for clarity. (b) Raman spectra of the pristine (black) and functionalized (red) samples of the L-GNR@SWCNTs, recorded under the excitation energy of 1.58 eV.

Similar trend can be observed when the concentration is increased to 100 mM except for a faster rate of reaction (Supporting Information Figure S10). The results provide strong evidence that the GNRs are well protected within the one-dimensional confined nanospace, without inducing diazonium reaction.

CONCLUSIONS

In conclusion, the extended, ultrathin GNRs with defined structures are synthesized inside the carbon nanotubes. The GNRs exhibit intense optical absorption peaks (E_{11} and E_{22}) at 1.5 and 3.4 eV, qualitatively consistent with the first-principles calculations. Since these flimsy nanoribbon structures may well be fragile, the presence of the outer sheaths allows surface modification to add new functionalities without compromising the properties of the inner GNRs. Structures of the GNRs can be possibly tuned with a suitable choice of precursors and the template nanotubes.

MATERIALS AND METHODS

Fabrication of S-GNR@SWCNTs. S-GNR@SWCNTs, containing mixture of coronene-dimers and oligomers, were prepared *via* vapor phase encapsulation of coronene, as reported in our previous study.[22] In brief, 6 mg of the open-capped SWCNTs (diameter *ca.* 1.4−1.6 nm, Type SO, Meijo Nano Carbon) and 10 mg of the coronene powder (95%, TCI) were loaded, respectively, into the separate compartments of an H-type pyrex tube, degassed and sealed in an ampule (10^{-6} Torr). After heating at 450 °C for 48 h, the resulting carbon nanotubes were then washed with 50 mL of toluene, dried and stored.

Fabrication of L-GNR@SWCNTs. The sample was prepared by heating S-GNR@SWCNTs in vacuum (10^{-6} Torr) at 700 °C for 48 h to induce further polymerization among the molecules encapsulated.

Preparation of Sample Dispersion. Two milligrams of the sample (pristine SWCNTs, S-GNR@SWCNTs and L-GNR@SWCNTs) was dispersed in 10 mL of 1 wt % sodium cholate (SC, 98%, Kishida)/D_2O for 20 h by using a bath type sonicator (Nanoruptor NR-350, Cosmo Bio). The dispersant was centrifuged at 52 000 rpm using a swing bucket rotor (S52ST, Hitachi) for 1 h to exclude aggregated bundles and metal particles. Then, 80% of the supernatant was collected and the concentration was adjusted to 0.5 abs at 1000 nm with 1 wt % SC/D_2O solution.

Diazonium Functionalization. The reaction was conducted in reference to the procedure described by Piao *et al.*;[31] 20 μL of the freshly prepared 10 or 100 mM 4-bromobenzenediazonium tetrafluoroborate (96%, Sigma-Aldrich) in D_2O solution was added to a glass vial containing 5 mL of the desired sample solution. The addition was repeated after every 24 h and the reaction was monitored over a period of 4 days. Exposure to light was minimized by wrapping the glass vial with an aluminum foil. The mixture was constantly stirred at room temperature.

Absorption Measurements. Optical absorption spectra were recorded on JASCO V-570 UV/vis/NIR spectrophotometer.

Raman Characterizations. The measurements were conducted directly on the bucky papers (for the pristine samples) or thin films prepared from the functionalized samples. Basically, 0.8 mL of the reacted solution was sampled and added to 3.2 mL of ethanol to allow the precipitation of CNTs. The precipitate was collected by vacuum-filtration and washed with 10 mL of EtOH. To ensure a thorough cleaning of the sample, the precipitate was sonicated for 5 min in 2 mL of EtOH, filtered and washed with 10 mL of EtOH and deionized water, respectively. The resulting CNT-thin film was dried in air prior to the measurements.

The samples were excited using a Sapphire solid-state laser at 2.54 eV (488 nm), a helium−neon laser at 1.96 eV (633 nm), and a diode laser at 1.58 eV (785 nm). Raman spectra taken at 2.54 and 1.96 eV were recorded on a single monochromator (HR-800, Horiba Jobin Yvon) equipped with a charge-coupled device (CCD) detector, while the measurements at 1.58 eV were performed on a Renishaw inVia Raman microscope.

HRTEM Observations. A small amount of the sample was dispersed in ~1 mL of 1, 2-dichloroethane solution, dripped cast onto the carbon-coated copper grid and dried in vacuum.

C_s-HRTEM Observations. A cold field emission JEM-2100F equipped with a spherical aberration (C_s) corrector (the DELTA-corrector) was operated at 60 kV for the HRTEM imaging with high resolution and high contrast so that the electron-beam damage of the specimen is reduced as much as possible (the beam density during the observations is less than 50 000 electrons/(nm^2·s) or 0.8 C/(cm^2·s). The specimen was observed at 200 °C to remove amorphous carbons around CNTs. The C_s was set to less than 1 μm. A Gatan 894 CCD camera was used for digital recording of the HRTEM images. A sequence of HRTEM

images (20 frames) was recorded, with a 2 s exposure time for each. After drift compensation, some frames can be superimposed to increase the signal-to-noise (SN) ratio for display. HRTEM images are filtered by a low pass filter after being filtered by a commercial software named HREM-Filters Pro. The simulation of HRTEM images is performed by using Mactempas software.

Computational Methods. First-principles total energy calculations were performed on the optimized geometries using DFT. LDA was adopted to account for the exchange-correlation interactions of electrons. Norm-conserving pseudo potentials were adopted to describe electron−ion interactions. The valence wave functions were expanded by the plane-wave basis set with the cutoff energy of 50 Ry.

Conflict of Interest: The authors declare no competing financial interest.

Acknowledgment. This work was supported by the Grant-in-Aid for Scientific Research S (No. 22225001) of MEXT, Japan. H.E.L. thanks JSPS for the Grant-in-Aid for JSPS Fellows and the support from IGER program. H.E.L. thanks Prof. Kenichiro Itami for the use of Renishaw Raman microscope. Y.M. acknowledges the financial support by a Grant-in-Aid for Young Scientist (B) (No. 24750180) and for Scientific Research on Innovative Areas (No. 26107530) of MEXT, Japan. S.O. thanks the financial support by CREST-JST. Z.L. acknowledges support from the MEXT KAKENHI "Science of Atomic Layers" (Grant Number 25107003). Z.L. and K.S. acknowledge support from a JST Research Acceleration Program. Arifin was supported by fellowships from the Nagoya University G30 and IGER programs.

Supporting Information Available: HRTEM images of the S-GNR@SWCNTs and L-GNR@SWCNTs. Simulated C_s-HRTEM images of L-GNR@SWCNTs. Raman spectra of the L-GNR@SWCNTs taken at 1.58, 1.96, 2.54 eV. Simulated Raman spectra of zigzag-edge GNRs with different lengths. Optical absorption and Raman spectra of the SWCNTs, S-GNR@SWCNTs and L-GNR@SWCNTs recorded over the course of reaction with 10 mM diazonium solution. Optical absorption of the SWCNTs, S-GNR@SWCNTs and L-GNR@SWCNTs recorded over the course of reaction with 100 mM diazonium solution. This material is available free of charge *via* the Internet at http://pubs.acs.org.

REFERENCES AND NOTES

1. Koch, M.; Ample, F.; Joachim, C.; Grill, L. Voltage-Dependent Conductance of a Single Graphene Nanoribbon. *Nat. Nanotechnol.* **2012**, *7*, 713–717.
2. Jensen, S. A.; Ulbricht, R.; Narita, A.; Feng, X.; Müllen, K.; Hertel, T.; Turchinovich, D.; Bonn, M. Ultrafast Photoconductivity of Graphene Nanoribbons and Carbon Nanotubes. *Nano Lett.* **2013**, *13*, 5925–5930.
3. Narita, A.; Feng, X.; Hernandez, Y.; Jensen, S. A.; Bonn, M.; Yang, H.; Verzhbitskiy, I. A.; Casiraghi, C.; Hansen, M. R.; Koch, A. H. R.; et al. Synthesis of Structurally Well-Defined and Liquid-Phase-Processable Graphene Nanoribbons. *Nat. Chem.* **2014**, *6*, 126–132.
4. Vo, T. H.; Shekhirev, M.; Kunkel, D. A.; Morton, M. D.; Berglund, E.; Kong, L.; Wilson, P. M.; Dowben, P. A.; Enders, A.; Sinitskii, A. Large-Scale Solution Synthesis of Narrow Graphene Nanoribbons. *Nat. Commun.* **2014**, *5*, 3189.
5. Denk, R.; Hohage, M.; Zeppenfeld, P.; Cai, J.; Pignedoli, C. A.; Söde, H.; Fasel, R.; Feng, X.; Müllen, K.; Wang, S.; et al. Exciton-Dominated Optical Response of Ultra-Narrow Graphene Nanoribbons. *Nat. Commun.* **2014**, *5*, 4253.
6. Chernov, A. I.; Fedotov, P. V.; Talyzin, A. V.; Suarez Lopez, I.; Anoshkin, I. V.; Nasibulin, A. G.; Kauppinen, E. I.; Obraztsova, E. D. Optical Properties of Graphene Nanoribbons Encapsulated in Single-Walled Carbon Nanotubes. *ACS Nano* **2013**, *7*, 6346–6353.
7. Fujita, M.; Wakabayashi, K.; Nakada, K.; Kusakabe, K. Peculiar Localized State at Zigzag Graphite Edge. *J. Phys. Soc. Jpn.* **1996**, *65*, 1920.
8. Nakada, K.; Fujita, M.; Dresselhaus, G.; Dresselhaus, M. S. Edge State in Graphene Ribbons: Nanometer Size Effect and Edge Shape Dependence. *Phys. Rev. B* **1996**, *54*, 17954–17961.
9. Son, Y.-W.; Cohen, M. L.; Louie, S. G. Energy Gaps in Graphene Nanoribbons. *Phys. Rev. Lett.* **2006**, *97*, 216803.
10. Yang, L.; Park, C.-H.; Son, Y.-W.; Cohen, M. L.; Louie, S. G. Quasiparticle Energies and Band Gaps in Graphene Nanoribbons. *Phys. Rev. Lett.* **2007**, *99*, 186801.
11. Li, X.; Wang, X.; Zhang, L.; Lee, S.; Dai, H. Chemically Derived, Ultrasmooth Graphene Nanoribbon Semiconductors. *Science* **2008**, *319*, 1229–1232.
12. Campos-Delgado, J.; Romo-Herrera, J. M.; Jia, X.; Cullen, D. A.; Muramatsu, H.; Kim, Y. A.; Hayashi, T.; Ren, Z.; Smith, D. J.; Okuno, Y.; et al. Bulk Production of a New Form of sp^2 Carbon: Crystalline Graphene Nanoribbons. *Nano Lett.* **2008**, *8*, 2773–2778.
13. Jiao, L.; Zhang, L.; Wang, X.; Diankov, G.; Dai, H. Narrow Graphene Nanoribbons from Carbon Nanotubes. *Nature* **2009**, *458*, 877–880.
14. Kosynkin, D. V.; Higginbotham, A. L.; Sinitskii, A.; Lomeda, J. R.; Dimiev, A.; Price, B. K.; Tour, J. M. Longitudinal Unzipping of Carbon Nanotubes to Form Graphene Nanoribbons. *Nature* **2009**, *458*, 872–876.
15. Elias, A. L.; Botello-Méndez, A. R.; Meneses-Rodríguez, D.; Jehová González, V.; Ramírez-González, D.; Ci, L.; Muñoz-Sandoval, E.; Ajayan, P. M.; Terrones, H.; Terrones, M. Longitudinal Cutting of Pure and Doped Carbon Nanotubes to Form Graphitic Nanoribbons Using Metal Clusters as Nanoscalpels. *Nano Lett.* **2009**, *10*, 366–372.
16. Cai, J.; Ruffieux, P.; Jaafar, R.; Bieri, M.; Braun, T.; Blankenburg, S.; Muoth, M.; Seitsonen, A. P.; Saleh, M.; Feng, X.; et al. Atomically Precise Bottom-up Fabrication of Graphene Nanoribbons. *Nature* **2010**, *466*, 470–473.
17. Yang, X.; Dou, X.; Rouhanipour, A.; Zhi, L.; Räder, H. J.; Müllen, K. Two-Dimensional Graphene Nanoribbons. *J. Am. Chem. Soc.* **2008**, *130*, 4216–4217.
18. Chuvilin, A.; Bichoutskaia, E.; Gimenez-Lopez, M. C.; Chamberlain, T. W.; Rance, G. A.; Kuganathan, N.; Biskupek, J.; Kaiser, U.; Khlobystov, A. N. Self-Assembly of a Sulphur-Terminated Graphene Nanoribbon within a Single-Walled Carbon Nanotube. *Nat. Mater.* **2011**, *10*, 687–692.
19. Wang, Z.; Li, H.; Liu, Z.; Shi, Z.; Lu, J.; Suenaga, K.; Joung, S.-K.; Okazaki, T.; Gu, Z.; Zhou, J.; et al. Mixed Low-Dimensional Nanomaterial: 2D Ultranarrow MoS_2 Inorganic Nanoribbons Encapsulated in Quasi-1D Carbon Nanotubes. *J. Am. Chem. Soc.* **2010**, *132*, 13840–13847.
20. Lim, H. E.; Miyata, Y.; Kitaura, R.; Nishimura, Y.; Nishimoto, Y.; Irle, S.; Warner, J. H.; Kataura, H.; Shinohara, H. Growth of Carbon Nanotubes *via* Twisted Graphene Nanoribbons. *Nat. Commun.* **2013**, *4*, 2548.
21. Talyzin, A. V.; Anoshkin, I. V.; Krasheninnikov, A. V.; Nieminen, R. M.; Nasibulin, A. G.; Jiang, H.; Kauppinen, E. I. Synthesis of Graphene Nanoribbons Encapsulated in Single-Walled Carbon Nanotubes. *Nano Lett.* **2011**, *11*, 4352–4356.
22. Fujihara, M.; Miyata, Y.; Kitaura, R.; Nishimura, Y.; Camacho, C.; Irle, S.; Iizumi, Y.; Okazaki, T.; Shinohara, H. Dimerization-Initiated Preferential Formation of Coronene-Based Graphene Nanoribbons in Carbon Nanotubes. *J. Phys. Chem. C* **2012**, *116*, 15141–15145.
23. Chamberlain, T. W.; Biskupek, J.; Rance, G. A.; Chuvilin, A.; Alexander, T. J.; Bichoutskaia, E.; Kaiser, U.; Khlobystov, A. N. Size, Structure, and Helical Twist of Graphene Nanoribbons Controlled by Confinement in Carbon Nanotubes. *ACS Nano* **2012**, *6*, 3943–3953.
24. Green, A. A.; Hersam, M. C. Processing and Properties of Highly Enriched Double-Wall Carbon Nanotubes. *Nat. Nanotechnol.* **2009**, *4*, 64–70.
25. Miyata, Y.; Suzuki, M.; Fujihara, M.; Asada, Y.; Kitaura, R.; Shinohara, H. Solution-Phase Extraction of Ultrathin Inner Shells from Double-Wall Carbon Nanotubes. *ACS Nano* **2010**, *4*, 5807–5812.
26. Strano, M. S.; Dyke, C. A.; Usrey, M. L.; Barone, P. W.; Allen, M. J.; Shan, H.; Kittrell, C.; Hauge, R. H.; Tour, J. M.; Smalley, R. E. Electronic Structure Control of Single-Walled Carbon Nanotube Functionalization. *Science* **2003**, *301*, 1519–1522.

27. Dyke, C. A.; Tour, J. M. Unbundled and Highly Functionalized Carbon Nanotubes from Aqueous Reactions. *Nano Lett.* **2003**, *3*, 1215–1218.
28. Schmidt, G.; Gallon, S.; Esnouf, S.; Bourgoin, J.-P.; Chenevier, P. Mechanism of the Coupling of Diazonium to Single-Walled Carbon Nanotubes and Its Consequences. *Chem.—Eur. J.* **2009**, *15*, 2101–2110.
29. Piao, Y.; Meany, B.; Powell, L. R.; Valley, N.; Kwon, H.; Schatz, G. C.; Wang, Y. Brightening of Carbon Nanotube Photoluminescence through the Incorporation of sp^3 Defects. *Nat. Chem.* **2013**, *5*, 840–845.
30. Tsyboulski, D. A.; Hou, Y.; Fakhri, N.; Ghosh, S.; Zhang, R.; Bachilo, S. M.; Pasquali, M.; Chen, L.; Liu, J.; Weisman, R. B. Do Inner Shells of Double-Walled Carbon Nanotubes Fluoresce?. *Nano Lett.* **2009**, *9*, 3282–3289.
31. Piao, Y.; Chen, C.-F.; Green, A. A.; Kwon, H.; Hersam, M. C.; Lee, C. S.; Schatz, G. C.; Wang, Y. Optical and Electrical Properties of Inner Tubes in Outer Wall-Selectively Functionalized Double-Wall Carbon Nanotubes. *J. Phys. Chem. Lett.* **2011**, *2*, 1577–1582.
32. Okazaki, T.; Iizumi, Y.; Okubo, S.; Kataura, H.; Liu, Z.; Suenaga, K.; Tahara, Y.; Yudasaka, M.; Okada, S.; Iijima, S. Coaxially Stacked Coronene Columns inside Single-Walled Carbon Nanotubes. *Angew. Chem.* **2011**, *123*, 4955–4959.
33. Okazaki, T.; Okubo, S.; Nakanishi, T.; Joung, S.-K.; Saito, T.; Otani, M.; Okada, S.; Bandow, S.; Iijima, S. Optical Band Gap Modification of Single-Walled Carbon Nanotubes by Encapsulated Fullerenes. *J. Am. Chem. Soc.* **2008**, *130*, 4122–4128.
34. Lempka, H. J.; Obenland, S.; Schmidt, W. The Molecular Structure of Boente's "Dicoronylene", as Deduced from PE and UV Spectroscopy. *Chem. Phys.* **1985**, *96*, 349–360.
35. Zhu, Y.; Higginbotham, A. L.; Tour, J. M. Covalent Functionalization of Surfactant-Wrapped Graphene Nanoribbons. *Chem. Mater.* **2009**, *21*, 5284–5291.
36. Perdew, J. P.; Levy, M. Physical Content of the Exact Kohn-Sham Orbital Energies: Band Gaps and Derivative Discontinuities. *Phys. Rev. Lett.* **1983**, *51*, 1884–1887.
37. Seidl, A.; Görling, A.; Vogl, P.; Majewski, J. A.; Levy, M. Generalized Kohn-Sham Schemes and the Band-Gap Problem. *Phys. Rev. B* **1996**, *53*, 3764–3774.
38. Prezzi, D.; Varsano, D.; Ruini, A.; Marini, A.; Molinari, E. Optical Properties of Graphene Nanoribbons: The Role of Many-Body Effects. *Phys. Rev. B* **2008**, *77*, 041404.